A Phenology-Dependent Analysis for Identifying Key Drought Indicators for Crop Yield based on Causal Inference and Information Theory

Özlem Baydaroğlu[1,*,+], Serhan Yeşilköy[2,3,4,+], Ibrahim Demir[1,5,6]

[1] IIHR – Hydroscience & Engineering, University of Iowa, Iowa, USA
[2] İstanbul Provincial Directorate of Agriculture and Forestry, Ministry of Agriculture and Forestry, İstanbul, Türkiye
[3] Oak Ridge Institute for Science and Education, Oak Ridge, Tennessee, USA
[4] USDA-ARS, Adaptive Cropping Systems Laboratory, Beltsville, Maryland, USA
[5] Civil and Environmental Engineering, University of Iowa, Iowa, USA
[6] Electrical and Computer Engineering, University of Iowa, Iowa, USA
*Corresponding Author: Ö. Baydaroğlu (ozlem-baydaroglu@uiowa.edu)
[+] Özlem Baydaroğlu and Serhan Yeşilköy equally contributed to this study.

Abstract

Drought indicators, which are quantitative measurements of drought severity and duration, are used to monitor and predict the risk and effects of drought, particularly in relation to the sustainability of agriculture and water supplies. This research uses causal inference and information theory to discover the drought index, which is the most efficient indicator for agricultural productivity and a valuable metric in estimating and predicting crop yield. The causal connection between precipitation, maximum air temperature, drought indices and corn and soybean yield is ascertained by cross convergent mapping (CCM), while the information transfer between them is determined through transfer entropy (TE). This research is conducted on rainfed agricultural lands in Iowa, considering the phenological stages of crops. Based on the nonlinearity analysis conducted using S-map, it is determined that causality analysis could not be carried out using CCM due to the absence of nonlinearity in the soybean yield data. The results are intriguing as they uncover both the causal connection between corn yield and precipitation and maximum temperature indices. Based on the analysis, the drought indices with the strongest causal relationship to crop production are SPEI-9m and SPI-6m during the silking period, and SPI-9m and SPI-6m during the doughing period. Therefore, these indices may be considered as the most effective predictors in crop yield prediction models. The study highlights the need of considering phenological periods when estimating crop production, as the causal relationship between corn yield and drought indices differs for the two phenological periods.

Keywords: Causal inference, Extreme Events, Corn, Soybean, Cross Convergent Mapping, Transfer Entropy

1. Introduction

Hydroclimatic disasters account for approximately 74% of all natural disasters (UNESCO, 2020). The cumulative drought-related damage nationwide since 1980 amounts to $44.8 billion, with the State of Iowa alone experiencing a total of $23.3 billion in prolonged drought damage in 1988 and 2012 (EM-DAT, 2024). Associated with climate change as the air temperature rises by 1°C, the atmosphere can store 6-7 percent more water, according to the Clausius-Clapeyron thermodynamics equation (Allen and Ingram, 2002). Rising air temperatures have accelerated the hydrological cycle (Tabari, 2020), which in turn has increased the frequency and severity of extreme weather events like droughts (AghaKouchak et al., 2020).

The Intergovernmental Panel on Climate Change (IPCC) defines compound events as either the occurrence of two or more extreme events happening at the same time or in succession, the combination of extreme events with underlying conditions that intensify their impact, or the combination of events that are not extreme on their own but result in an extreme event or impact when combined (Seneviratne et al., 2012). Climate change leads to a rise in the frequency and severity of hydroclimatic extremes like heat and cold waves, droughts, and floods (Baydaroğlu and Demir, 2024; Alabbad et al., 2024) and compound events (Leonard et al., 2014; Messmer and Simmonds, 2021; Yeşilköy and Baydaroğlu, 2024). Hydroclimatic extremes, particularly droughts like agricultural, hydrological (Yeşilköy and Şaylan, 2022) and snow drought (Yeşilköy et al., 2024) have been associated with particularly poor harvests (up to 30% yield losses) in regions including India, Ethiopia, the US, Europe, and Russia, as revealed by Lesk et al. (2022).

According to Van Vliet et al. (2023), droughts and heatwaves decrease dissolved oxygen, increase river temperature, algae, salinity, and pollutant concentrations due to reduced dilution, while also lowering pollutant transport from agricultural and urban runoff. Wang et al. (2023) examined compound wet-heatwave events, as well as compound droughts and heatwaves, utilizing maximum air temperature (T_{max}) and the self-calibrated Palmer drought severity index (scPDSI). Vogel et al. (2021) employ the least absolute shrinkage and selection operator (LASSO) and use annual wheat yield data to investigate crop failure. The compounding effects of both meteorological variables and various periods of the growing season in the formation of crop failure events is demonstrated by their study results. The impact of heatwaves, drought, and extreme precipitation on yield variability during the growing season for maize was examined by Simanjuntak et al. (2023) through the use of stress indices and Peter and Clark Momentary Conditional Independence (PCMCI) (Runge et al., 2015). The study indicates that heatwaves exacerbated drought conditions, however no causal relationship between heatwaves and extreme precipitation was found.

Tewari et al. (2015) used the Granger causality (GC) to identify climate factors responsible for fluctuations in soybean prices. The study's findings demonstrated a clear causative relationship between fluctuations in soybean commodity prices and precipitation, whereas no causal link was observed between air temperature and soybean prices. Lu et al. (2024) employed the PCMCI method to differentiate the impact of vapor pressure deficit (VPD) and soil moisture on vegetation response. The results indicate that insufficient soil moisture and a high VPD are restricting factors

for the growth of vegetation. The VPD was shown to have a positive causal effect of 48% and a negative causal effect of 52% on the Normalized Differential Vegetation Index (NDVI) across the entire area.

Studies also apply information theory to causality and predictability discovery. Kimm et al. (2020) employed data from eddy covariance stations, two statistical models, and information theory to measure the relationship between gross primary production (GPP), VPD, and soil water content in rainfed corn and soybean fields located in the US Corn Belt. Their findings demonstrated that 91% of the fluctuation in GPP may be linked to changes in VPD. A study by Zhu et al. (2023) utilized a transfer entropy (TE) method and new network parameters to uncover the trends and strengths of the interaction between land and atmosphere. They examined both historical conditions and a future scenario with high emissions. In observations, it was discovered that the current extratropical forest coupling network has a significant degree of network connectedness.

While numerous studies have investigated the correlation between meteorological factors and crop yields in the US, particularly in the Corn Belt - a prominent region in the Midwest known for corn and soybean cultivation - there is a scarcity of research on causality. The following are some of the studies that have been conducted on the yield of maize and soybeans: Ting et al. (2023) employed a multiple regression model using observational data to demonstrate that extreme dry heat significantly decreased corn and soybean yields in the US. However, humid heat extremes had negligible effects and even enhanced yields in certain regions, despite having similar high dry-bulb temperatures as the dry heat conditions.

Keppenne (1995) conducted a study using a 48-month time span and using a multi-channel single spectrum analysis approach to identify a correlation between El Niño–Southern Oscillation (ENSO) and soybean prices. Nevertheless, no correlation with causality was identified, which is consistent with the research conducted by Letson and McCullough (2001), which employed GC (Zhu and Ghoshray, 2021). Cambron et al. (2024) investigate the effects of conservation tillage on maize productivity in the western part of Corn Belt using high resolution satellite data on tillage techniques and crop yields, and causal forest analysis. They discovered that over time, conservation tillage improved rainfed maize yields in the area by 9.9%.

In order to model extreme air temperature and precipitation indices, Wilson et al. (2022) assessed the performance of 32 downscaled models from the Localized Constructed Analogs (LOCA) of the 5th Coupled Model Intercomparison Project (CMIP5) of the US Global Change Research Program. The findings highlight several important regional trends, including rising extreme minimum air temperatures, falling daily air temperature ranges, rising warm nights and decreasing cold nights. According to Sun et al. (2023), a modified version of the GLYCIM soybean model predicts that the number of hot days that have a negative impact on soybean yield will increase in the US Midwest. In their study, Feng et al. (2015) found that a 1% change in yields in rural counties of the Corn Belt is associated with a corresponding decrease of 0.3-0.4 percentage points in the net migration rate.

Research on the connections between climate variability and agricultural sustainability, and subsequent migration, is crucial due to its significant influence. This study investigates the effects

of precipitation and T_{max} on agriculture by analyzing data on both variables as well as drought indices, with a focus on causality. The paper is structured as follows: Section 2 explains the study area, data, CCM method. The causal relationships and correlation values among meteorological variables and conclusions can be found in sections 3 and 4.

2. Materials and Methods

2.1. Study Area

State of Iowa is located in the Corn Belt, which is a dominant region in the Midwestern US for corn production. Approximately 92% of the cropland in the US Corn Belt relies on precipitation and is very susceptible to yearly fluctuations in climate as well as potential future climatic shifts (Kimm et al., 2020). According to the US National Agricultural Statistics Service (NASS), the state possesses approximately 13 million acres of cornfields and 9 million acres of soybean fields. Iowa holds the top position in agricultural production in the US. Most residents rely on agriculture as their primary source of income, and more than 85% of its land is dedicated to agricultural activities (USDA-ERS, 2024). Iowa has encountered significant droughts and substantial flood damage in both urban and agricultural regions (Yildirim et al., 2023; Cikmaz et al., 2023). Despite being one of the states with the lowest social vulnerability in its agricultural communities (Tanir et al., 2024), it is evident that the drought (Yeşilköy et al., 2023; Islam et al., 2024) and flood related challenges (Yildirim et al., 2022; Li and Demir, 2022; Alabbad et al., 2023) in recent years have an impact on agricultural productivity in Iowa. Figure 1 shows nine agricultural districts of Iowa.

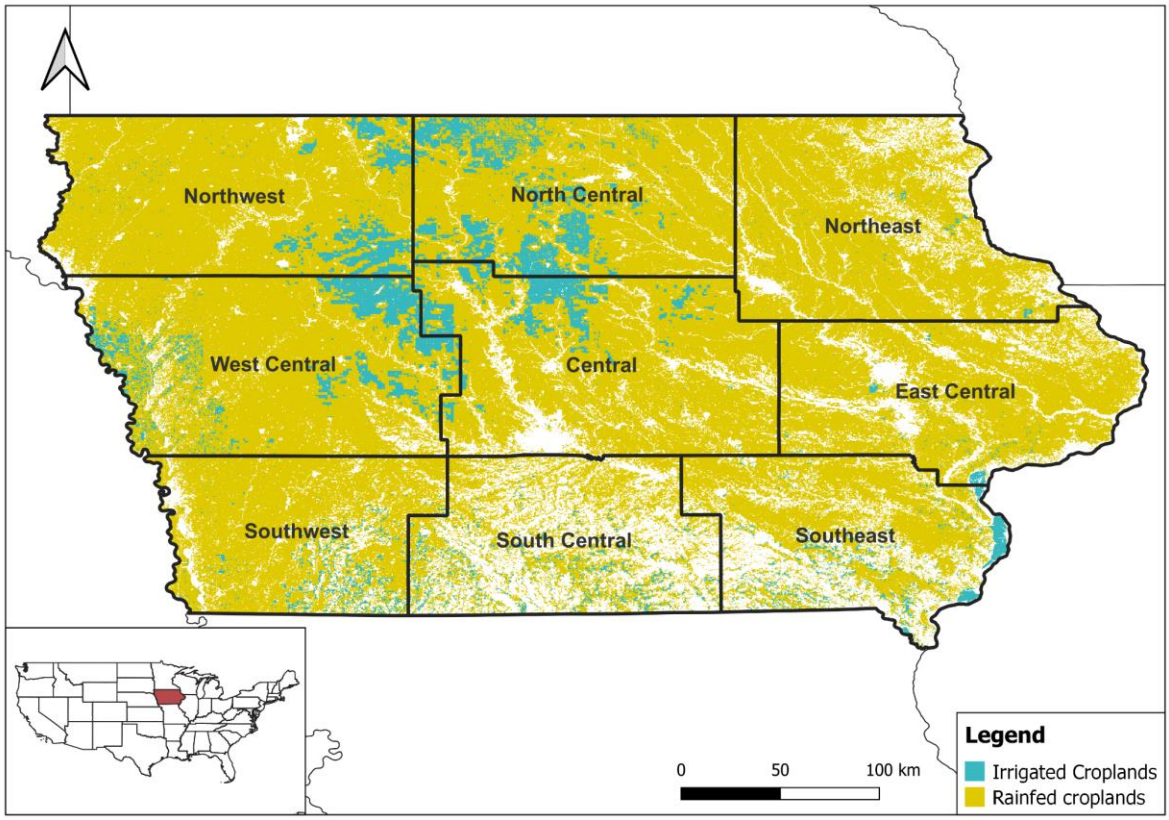

Figure 1. The State of Iowa has nine agricultural districts (USDA-NASS) as groups of counties within states that are grouped by geography, climate, and cropping practices. Based on the Landsat-Derived Global Rainfed and Irrigated-Cropland Product (LGRIP) data, most agricultural lands are non-irrigated. The USDA's census of agriculture also states irrigated cropland is less than 1% (USDA-ERS, 2024).

2.2. Study Data

In this study, daily T_{max} (°C) and precipitation (mm) data were downloaded from DAYMET, which provides long-term, gridded dataset with 1-km resolution for North America. Gridded drought indices Evaporative Demand Drought Index (EDDI), scPDSI, Standardized Precipitation and Evapotranspiration Index (SPEI), Standardized Precipitation Index (SPI) with different monthly scales data at 4-km spatial resolution were obtained from gridMET on a daily scale across the contiguous US. Crop (corn and soybean) phenological data were extracted from USDA-NASS database for the entire Iowa. While extracting the meteorological data according to phenological periods, which were selected from the beginning of the phenological period in the agricultural areas across the state as the period when they were seen in at least 80% of the state. Silking and doughing, blooming and setting pods were selected for corn and soybean, respectively. These reproductive stages are the most vulnerable periods to water stress, causing yield reduction and poor grain fill (Romano et al., 2011; Yang et al., 2021; Soba et al., 2022; Veas et al., 2022).

Even when data from multiple years are used, the amount of data is still minimal because temporal resolution of yield data is annual. Therefore, rather than assessing each agricultural

district individually, the data from all districts has been combined and employed in the study. In other words, a state-level assessment was conducted. During the data organization process, data from all districts was merged, considering both geography and time. Put simply, the data from 2005 to 2023 has been combined, considering the geographical proximity from the northwest (NE) agricultural district to the southeast agricultural district (SE). The reason for this is that climatic effects are influenced by factors such as latitude, longitude, topographic similarities, active synoptic patterns, and temporal evolution.

Figure 2 displays corn yields based on agricultural districts, whereas Figure 3 presents soybean yields based on the same districts. According to Figure 2, the production of corn has increased in every agricultural district between the years 2005 and 2023. In particular, the west central and southwest districts have grown faster than the other districts. In 2012, some parts of the state were affected by an extreme drought event, which occurred in the Upper Mississippi River Basin (Yeşilköy et al., 2024, Mount et al., 2024). The yield decrease in the southern agricultural districts was calculated as 26%. Moreover, all districts saw a sharp decline (30.1% yield reduction) in corn yield in 2020 because of a nationwide extreme drought event across the US (LeComte, 2021), which was quickly followed by sharp increases in 2021 and 2022.

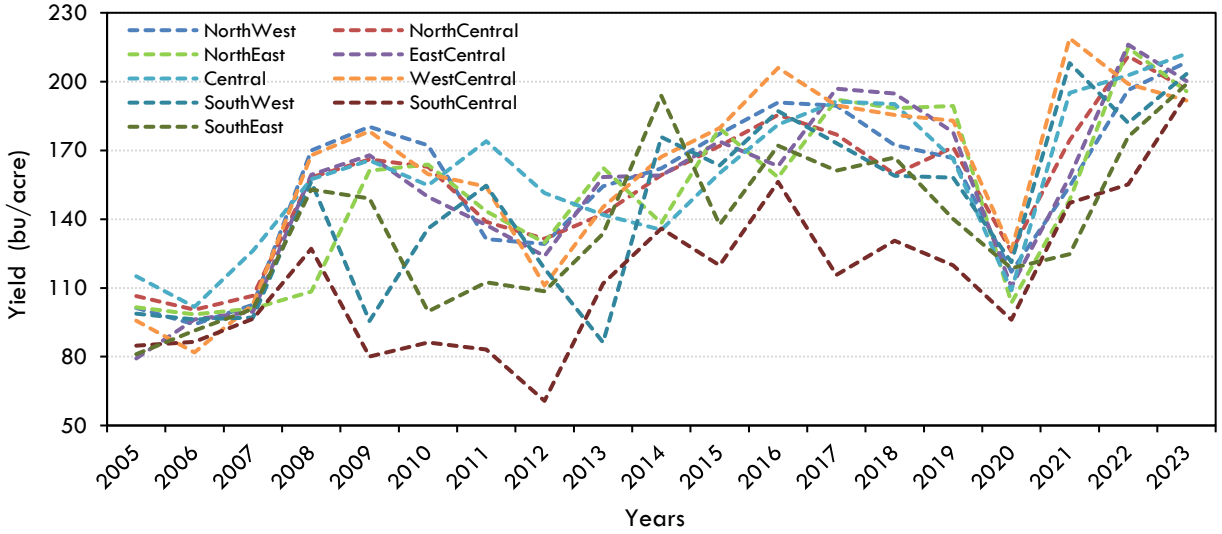

Figure 2. Corn yields of Iowa are based on nine agricultural districts.

As seen in Figure 3, soybean yield showed an upward trend in all districts from 2005 to 2023. However, the east central and southeast districts experienced the biggest increase. The upward trends observed in 2008, 2012, and 2020, as well as the downward trends observed in 2011, 2016, and 2021, are clearly apparent. Figures 4 and 5 show the mean precipitation and T_{max} during the crop growing season for corn and soybean crops. The phenological stages of these two crops coincide with the same months of the year.

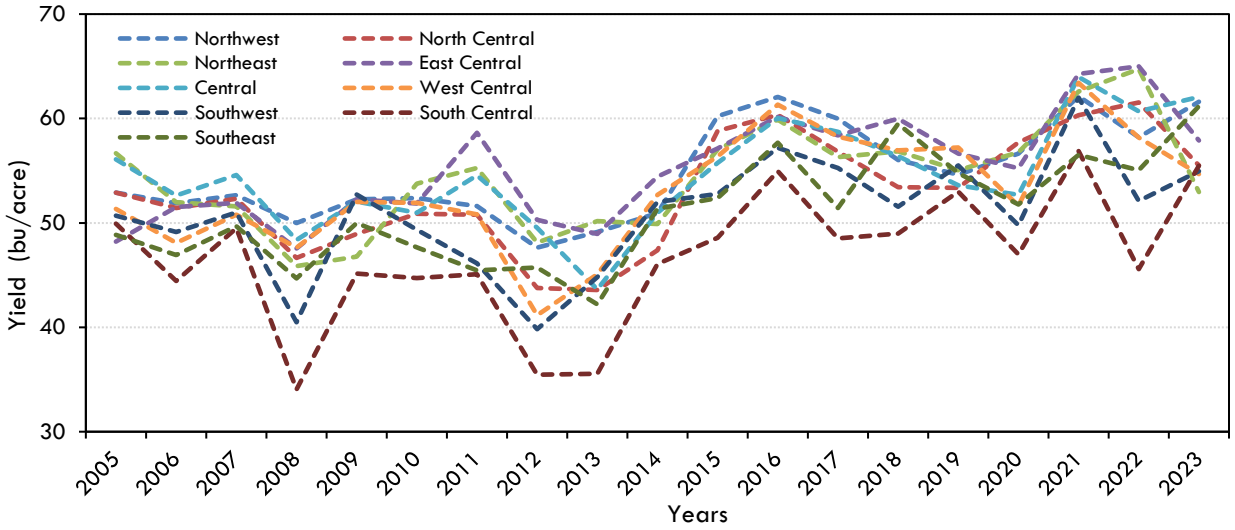

Figure 3. Soybean yields of Iowa are based on nine agricultural districts.

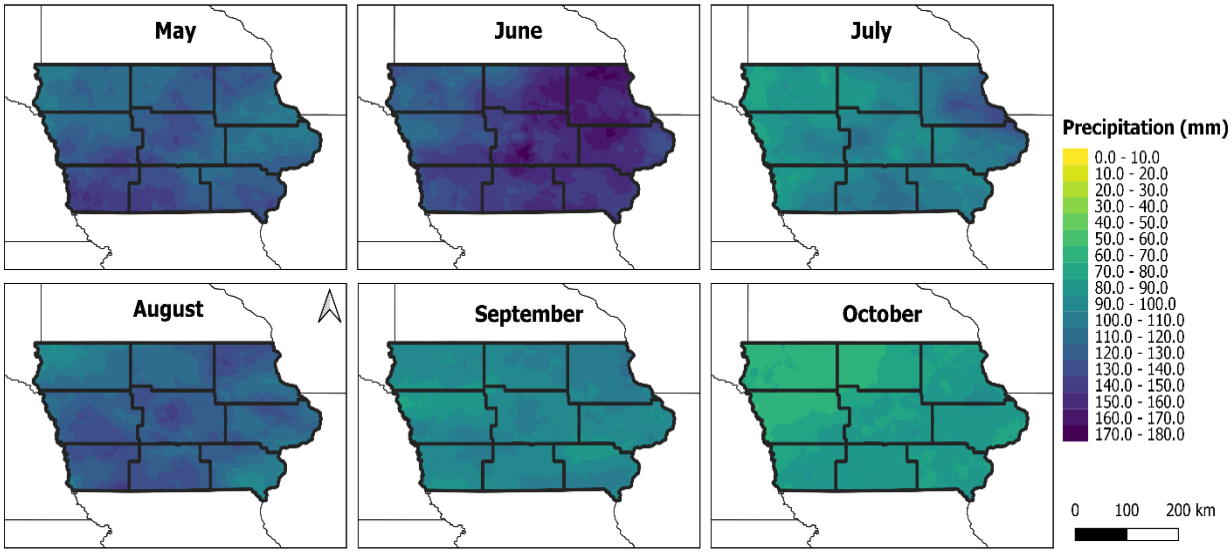

Figure 4. Distribution of Iowa's precipitation by months.

Figure 4 shows that the highest precipitation occurs in June (mean value is 144.8 mm across the state), especially in the east and northeast of Iowa. The total rainfall in Iowa during the months of May through October is calculated as 663.6 mm. The mean total rainfall in July (99.3 mm) and August (121.6 mm), when crops are in their regenerative phenological stages, is 220.9 mm.

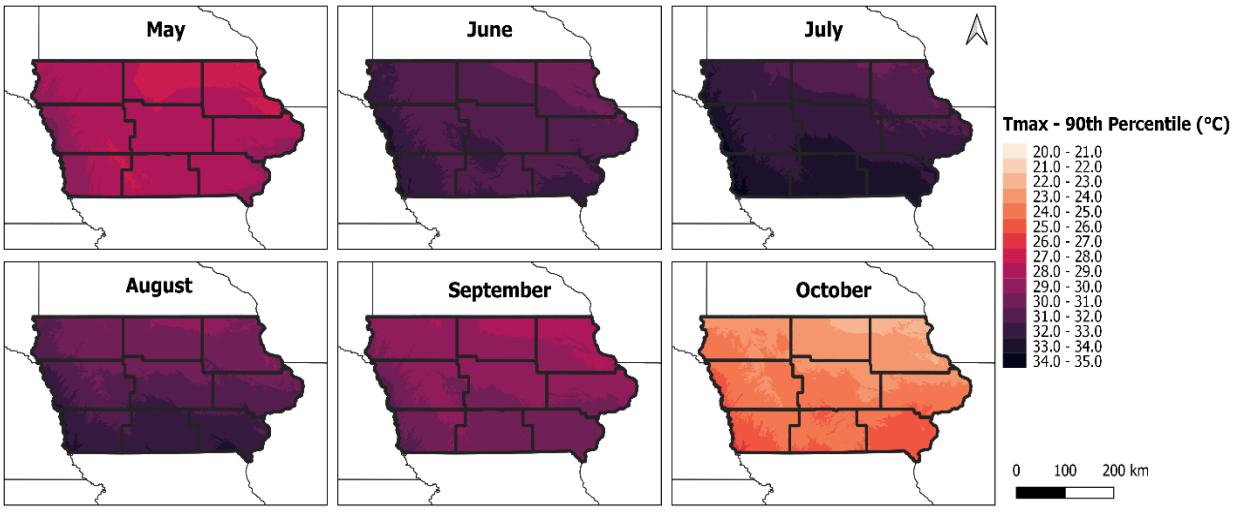

Figure 5. Distribution of Iowa's T_{max} by months.

Figure 5 illustrates that the southern regions of Iowa encounter high air temperatures. The mean T_{max} between May and October is calculated as 29.7°C throughout the state. The hottest month, July, has the state's average value of 32.5°C. This value reaches 34.7°C in the southern part of the state. Also, the mean value of the T_{max} in July does not fall below 30°C. The mean value of T_{max} in August ranges from 29.2 to 33.6°C, with a mean across the state of 31.4°C.

2.3. Cross Convergent Mapping (CCM)

CCM is a method that utilizes phase space reconstruction and has the ability to differentiate between causality and correlation. This reconstruction allows for the identification and measurement of causation through cross-mapping prediction. Reconstructing the phase space is essential for assessing the complexity of the system's attractor and the observed dynamic behaviors (Baydaroğlu and Koçak, 2014). The embedding theorem (Takens, 1981) allows for the construction of a phase space from a one-dimensional time series, determining the optimum embedding dimension and time delay (Baydaroğlu et al., 2018).

The underlying idea of CCM (Sugihara et al., 2012) is based on Takens' Theorem, which states that if there is a causal relationship between x and y, then the past values of x may be reconstructed solely from the variable y. CCM, which includes simplex projection, is a technique that is based on the embedding theorem. In phase space reconstruction, simplex projection is a nearest neighbor forecasting algorithm to follow the future trajectory of neighboring points (Sugihara and May, 1990; Hsieh et al., 2005). The optimal embedding dimension and time delay are determined through simplex projection. In a topological context, a neighborhood in M_x corresponds to a neighborhood in M_y. Here, M_x and M_y represent the shadow manifolds of the components of a deterministic process and the same dynamic system, denoted as X and Y, respectively (Bonotto et al., 2022). For the length of two components, $X(t)$ and $Y(t)$), L; delay time τ and the embedding dimension E, reconstruction procedure (Eq.1) can be given as,

$$X(t) = \langle x(t), x(t-\tau), x(t-2\tau), \ldots, x(t-(E-1)\tau \rangle \quad (1)$$

$$Y(t) = \langle y(t), y(t-\tau), y(t-2\tau), \dots, y(t-(E-1)\tau \rangle$$

shadow manifolds (Eq.2) are,

$$M_x = \{X(t), X(t-\tau), X(t-2\tau), \dots, X(t-(E-1)\tau\} \quad (2)$$
$$M_y = \{Y(t), Y(t-\tau), Y(t-2\tau), \dots, Y(t-(E-1)\tau\}$$

In order to make a single forecast at a certain time, E+1 nearest neighbors are determined in My based on their Euclidean distance to Y, taking into account a specific library size. The size of the library determines the length of the subsample of the shadow manifold My, which allows for the identification of nearest neighbors. The forecast of X $\left(\hat{X}\middle|My\right)$ is calculated by first mapping the points in X using the time indices of the nearest neighbors that have been found, and then averaging those points with respect to the Euclidean distances in My. The CCM cross-map skill is quantified as the Pearson's correlation between the observed X and forecasted $\left(\hat{X}\middle|My\right)$ for all time indices (Ye et al., 2015; Bonotto et al., 2022). Finally, a prediction model can be defined as

$$\left(\hat{X}\middle|My\right) = \sum_{i=1}^{E+1} w_i X(t_i) \quad (3)$$

where w_i indicates weights and they are calculated exponentially based on the Euclidean distance between $Y(t)$ and the nearest neighboring points, and $\|\cdot\|$ is the Euclidean norm in $\mathbb{R}^E$ (Mønster et al., 2017):

$$w_i = u_i \,/\, \sum_{j=1}^{E+1} u_j, u_i = exp\left(-\frac{\|Y(t)-Y(t_i)\|}{\|Y(t)-Y(t_1)\|}\right) \quad (4)$$

2.4. Transfer Entropy (TE)

TE is a distinct metric for quantifying the transfer of information, which is rooted in the principles of information theory (Shannon, 1948). Information theory ideas provide the foundation of TE. Two primary concepts underlie TE (Schreiber, 2000). The initial concept posits that entropy is derived from the stationary probability of states, while entropy rate is obtained from the transition probabilities. The second concept states that in the absence of information flow from Y to X, the transition probabilities of X remain unaltered, regardless of the historical data from Y (Sironen, 2020). Schreiber (2000) suggested using Markov processes to approximate the two time-series of interest, $X = x_t$ and $Y = y_t$ and then computing the deviation from the following generalized Markov condition as a measure of causation.

$$p(y_{t+1}|y_t^n, y_t^m) = p(y_{t+1}|y_t^n) \quad (5)$$

where $x_t^m = (x_t, \dots, x_{t-m+1})$, $y_t^n = (x_t, \dots, x_{t-n+1})$, m and n are the orders of X and Y's Markov processes, respectively. The TE from X to Y is estimated by calculating the expected Kullback-Leibler divergence (Kullback, 1951) between the probability distributions on each side of Equation

(5) in order to quantify causality (Vicente et al., 2011). The study utilized rEDM (Ye et al., 2016; Sugihara et al., 2020), RTransferEntropy and, causal-ccm (Javier, 2021) as R libraries and Python package, respectively.

$$TE\ (X \rightarrow Y) = \sum_{y_{t+1}, y_t^n, x_t^m} p(y_{t+1}, y_t^n, x_t^m) log\left(\frac{p\left(y_{t+1} \middle| y_t^n, x_t^m\right)}{p\left(\left(y_{t+1} \middle| y_t^n\right)\right.}\right) \quad (6)$$

3. Results and Discussions

Although the CCM method has some drawbacks, it also has certain advantages. Regarding the constraints, as noted in the research conducted by Bartsev et al. (2021) and Bonotto et al. (2022), spurious causality may result from seasonality and trends in the data, and the frequency of data sampling can also influence seasonality. These are undesirable attributes for the data to which CCM will be applied. Regarding the benefits of this method, CCM is able to determine the states across parameters. This approach avoids the risk of losing information due to chaotic dynamics and is capable of handling random factors. In addition, the primary characteristic of CCM that distinguishes it from simple correlation and points to causation is its convergence (Sugihara et al., 2012).

To investigate the impact of precipitation and T_{max} on corn and soybean yields, precipitation, T_{max} and drought indices which belong to phenological periods (July and August) have been used in order to capture both individual and compound effects, thereby eliminating or mitigating the influence of long-term trends and seasonalities. By ignoring pre-processing techniques like denoising (Baydaroğlu et al., 2024), detrending and deseasonalization, the potential loss of information in the data is avoided. Using the CCM approach, the study has investigated the causal relationship between corn and soybean yields and drought indices like, scPDSI, SPEI, SPI with different timescales (3-, 6-, 9-, 12-month) as hydroclimatic extreme events' indicators considering crop phenological periods.

During the initial phase of the investigation, with the simplex projection (Sugihara & May 1990), embedding dimensions ranging from 1 to 5 and time delays ranging from 1 to 7 have been tested to determine optimal values to reconstruct shadow manifolds. Across all data sets, the prediction horizon has been set to 1. The embedding dimension that resulted in the highest cross-mapping performance (the best prediction skill) has been selected. As seen in Table 1, the simplex projection analysis reveals consistent embedding dimension and time delay values across all drought indices and yield (Figures S1(a-o) for silking period and Figures S3(a-o) for doughing period). Table 2 shows the values of the embedding dimensions and time delays for every dataset, with the exception of the yield and precipitation pair for the soybean blossoming and setting pods periods, which are 2 and 1, respectively. During the blooming period, embedding dimensions and time delays for precipitation and yield are 4 and 1, whereas during the setting pods period, they are 4 and 4.

Table 1. Embedding dimensions, time delays and nonlinear parameters of all data sets for corn silking (period I) and doughing (period II) periods.

Period I For Y&	P	T_{max}	EDDI (3m)	EDDI (6m)	EDDI (9m)	EDDI (12m)	scPDSI	SPEI (3m)	SPEI (6m)	SPEI (9m)	SPEI (12m)	SPI (3m)	SPI (6m)	SPI (9m)	SPI (12m)
ED	2	2	2	2	2	2	2	2	2	2	2	2	2	2	2
TD	1	1	1	1	1	1	1	1	1	1	1	1	1	1	1
NP	5	1	1	1	1	1	1	1	1	1	1	1	1	1	1
Period II For Y&	P	T_{max}	EDDI (3m)	EDDI (6m)	EDDI (9m)	EDDI (12m)	scPDSI	SPEI (3m)	SPEI (6m)	SPEI (9m)	SPEI (12m)	SPI (3m)	SPI (6m)	SPI (9m)	SPI (12m)
ED	2	2	2	2	2	2	2	2	2	2	2	2	2	2	2
TD	1	1	1	1	1	1	1	1	1	1	1	1	1	1	1
NP	2	2	1	1	1	1	1	1	1	1	1	1	1	1	1

ED: Embedding dimension, TD: Time delay, NP: Nonlinear parameter, Y: Yield, P: Precipitation, T_{max}: Maximum air temperature

In simplex projection, a time delay of 1 is used to achieve the maximum resolution for embedding (Javier et al., 2022; Bonotto et al., 2022; Tian et al., 2024). Therefore, we have set the time delay to 1 since it provides for maximum resolution and is consistent with our findings. In the second phase of the study, the nonlinearity of all datasets has been determined using S-map (sequential locally weighted global linear map) (Figures S2(a-o) for silking period and S4(a-o) for doughing period). If the value of the nonlinear parameter at the point where the prediction skill reaches its highest level is zero, then the model is considered linear. However, if the value is more than zero, then the model is classified as nonlinear (Sugihara, 1994). Based on the S-map results, the datasets for corn in both phenological periods exhibit nonlinearity, whereas the datasets for soybean in both phenological periods lack nonlinearity. Hence, it is inappropriate to establish the causal connection between soybean yield and precipitation, maximum temperature, and drought indices using CCM.

Table 2. Embedding dimensions, time delays and nonlinear parameters of all data sets for soybean blooming (period I) and setting pods (period II) periods.

Period I For Y&	P	T_{max}	EDDI (3m)	EDDI (6m)	EDDI (9m)	EDDI (12m)	scPDSI	SPEI (3m)	SPEI (6m)	SPEI (9m)	SPEI (12m)	SPI (3m)	SPI (6m)	SPI (9m)	SPI (12m)
ED	4	2	2	2	2	2	2	2	2	2	2	2	2	2	2
TD	1	1	1	1	1	1	1	1	1	1	1	1	1	1	1
NP	0	0	0	0	0	0	0	0	0	0	0	0	0	0	0
Period II For Y&	P	T_{max}	EDDI (3m)	EDDI (6m)	EDDI (9m)	EDDI (12m)	scPDSI	SPEI (3m)	SPEI (6m)	SPEI (9m)	SPEI (12m)	SPI (3m)	SPI (6m)	SPI (9m)	SPI (12m)

ED	4	2	2	2	2	2	2	2	2	2	2	2	2	2	2
TD	4	1	1	1	1	1	1	1	1	1	1	1	1	1	1
NP	0	0	0	0	0	0	0	0	0	0	0	0	0	0	0

ED: Embedding dimension, TD: Time delay, NP: Nonlinear parameter, Y: Yield, P: Precipitation, T_{max}: Maximum air temperature

In the third phase of the investigation, the causal connection between the variables has been determined by employing CCM with a significance of $p < 0.05$. It is imperative to observe convergence in the prediction skill, which shows information transfer from the causal to the affected factor in order to differentiate between spurious causality and causality via CCM. This is accomplished by determining whether larger libraries generate cross-map skills that are progressively larger (Bonotto, 2022). In other words, causation is indicated by the prediction skill (ρ) increasing with library size and by its convergence to an extreme value (Tian et al., 2024). Table 3 displays the causality rates obtained using CCM, TE values, and Pearson correlation coefficients for all data sets. The highest values in Table 3 are shown by bold letters. The largest positive and negative correlation values are both displayed in bold in the correlation values. Furthermore, the data displayed as zero in the table are disregarded due to their significance value exceeding 0.05.

Table 3. Causality, TE, and correlation coefficient values for all data sets.

Periods	Corn - Silking			Corn - Doughing		
Criteria → Variables ↓	CCM	TE	Corr	CCM	TE	Corr
Yield & P	0.19	0.03	**0.14**	0.19	0.01	**0.18**
Yield & Tmax	**0.35**	0.03	**-0.41**	0.30	0.02	**-0.28**
Yield & EDDI-3m	0.30	0.02	-0.13	0.31	0.01	-0.14
Yield & EDDI-6m	0.26	0.01	-0.18	0.23	0.01	-0.17
Yield & EDDI-9m	0.26	0.01	-0.11	0.22	0.01	-0.14
Yield & EDDI-12m	0.27	0.01	-0.06	0.25	0.01	-0.08
Yield & ScPDSI	0.30	0.02	**0.14**	0.36	0.02	0.08
Yield & SPEI-3m	0.21	0.03	0.07	0.23	0.03	0.06
Yield & SPEI-6m	0.32	0.03	0.06	0.30	0.03	0.03
Yield & SPEI-9m	0.34	0.03	0.09	0.34	0.03	0.07
Yield & SPEI-12m	0.31	0.03	0.05	0.33	0.03	0.05
Yield & SPI-3m	0.20	0.04	0.05	0.24	0.03	0.03
Yield & SPI-6m	0.33	0.08	0.00	0.37	0.06	-0.04
Yield & SPI-9m	0.32	**0.12**	0.05	**0.39**	**0.09**	0.01
Yield & SPI-12m	0.32	0.02	0.06	0.35	0.02	0.06

The results of the analysis conducted using focusing causal inference to determine the impacts of the parameters on corn yield are as follows: Based on the CCM results, it can be concluded that the maximum temperature is the most influential factor (0.35) for corn yield during the *silking period*. The drought indices that have the strongest causal relationship with corn yield are SPEI-9m (0.34) and SPI-6m (0.33). The indicator that most accurately reflects causality during the *doughing period* is SPI-9m (0.39). Following this index, SPI-6m (0.37) and scPDSI (0.36) are also significant. The influence of phenological periods on the causality analysis results is clearly apparent.

According to the TE analysis, SPI-9m exhibits the highest level of information transfer, with a value of 0.12, during both the *silking* and *doughing periods*. This outcome aligns with the results obtained by the CCM. When looking at the correlation results, it is quite clear that causality and correlation are different phenomena. In the *silking period*, the strongest positive correlation (0.14) is between yield and precipitation and scPDSI datasets, while the highest negative correlation (-0.41) is between yield and maximum temperature. In the *doughing period*, the strongest positive correlation (0.18) is between yield and precipitation, while the highest negative correlation (-0.28) is between yield and maximum temperature.

4. Conclusion

Establishing causal relationships between meteorological variables and agricultural yield estimation, as well as constructing prediction models, is a highly complex and significant task. The main difficulties in doing causal analysis lie in the nonlinearity of meteorological data and the individual as well as combined impacts of hydrometeorological events. In accordance with this concept, a preliminary investigation has been conducted as a precursor to the development of a corn yield forecast model. Therefore, during the development of a corn yield prediction model, an effort has been made to identify the specific variables or drought indicators that should be incorporated into the model. Put simply, this study begins with the premise that variables with higher causality values defined by CCM have a greater capacity to accurately depict the relevant process.

The primary challenge in analyzing and conducting model studies on agricultural yield stems from the limited quantity of yield data available each year. Therefore, incorporating variables that will enhance yield data into models will greatly contribute to regarding efforts. The primary challenge of the CCM approach lies in the requirement for data that is devoid of trends, seasonality, and noise. To address this issue, the study focused on using a limited dataset consisting of only two months (for two periods) per year.

The benefits derived from the study can be briefly described as follows: (1) Development of prediction models that account for phenological periods is required to ensure prediction accuracy, since the causality values for the crop to be investigated or predicted vary according to these periods. (2) Our research, which involves the use of corn yield, meteorological variables, and drought indices, indicates that the causality between precipitation and yield is equivalent for both

periods, while the maximum temperature is more effective during the silking period, as indicated by the CCM results.

It is evident that SPEI-9m and SPI-6m are additional prominent indices during this period. In the doughing period, the variables that have shown the strongest connection with corn yield are SPI-9m, SPI-6m, and scPDSI, in that order. The fact that SPI-9m has the strongest causal relationship indicates the importance of the 9-month rainfall calculated during this period. In other words, although maximum temperature is the most essential component in the silking period, precipitation takes precedence in the doughing period. The TE results reveal that the SPI-9m contains the most significant information about corn yield in both periods. Given that SPIs are derived based on monthly intervals using precipitation data, both CCM and TE findings indicate that precipitation is the primary meteorological factor influencing corn production. Consequently, precipitation data should be assigned the greatest weight in corn yield models.

Furthermore, the results of this investigation indicate that indices with fewer variables, such as SPI, are more effective in capturing the process than more intricate and multivariate drought indices. SPI is a straightforward method for quantifying wet and dry periods. It allows for meaningful comparisons across different climatic conditions and relies just on precipitation data for its calculation (WMO, 2012; Öz et al., 2024). The development of a causality analysis method or a corn yield prediction model that takes into account lagged effects for causality analysis may be a significant advancement from this study. Due to the potential for meteorological variables to have a delayed impact on agriculture (Chen et al., 2020, Zhang and Wang, 2021).

5. Acknowledgement

The funding for this study was provided by the University of Iowa Interdisciplinary Scalable Solutions for a Sustainable Future Project under the grant title Watershed-Level Multicriteria Quantification of Agricultural Sustainability for Iowa. This research was supported in part by an appointment to the Agricultural Research Service (ARS) Research Participation Program administered by the Oak Ridge Institute for Science and Education (ORISE) through an interagency agreement between the U.S. Department of Energy (DOE) and the U.S. Department of Agriculture (USDA). ORISE is managed by ORAU under DOE contract number DE-SC001466. All opinions expressed in this paper are the author's and do not necessarily reflect the policies and views of USDA, DOE, or ORAU/ORISE.

6. Data Availability

Crop phenology data were extracted from here (USDA-NASS):
https://www.nass.usda.gov/Charts_and_Maps/Crop_Progress_&_Condition/index.php
Land Cover Map: https://lpdaac.usgs.gov/products/lgrip30v001/
Drought Indices (EDDI, scPDSI, SPEI, SPI): https://www.climatologylab.org/gridmet.html
Meteorological (Precipitation and T_{max}) Data: https://daymet.ornl.gov/

7. References

AghaKouchak, A., Chiang, F., Huning, L. S., Love, C. A., Mallakpour, I., Mazdiyasni, O., ... & Sadegh, M. (2020). Climate extremes and compound hazards in a warming world. *Annual Review of Earth and Planetary Sciences*, *48*(1), 519-548. https://doi.org/10.1146/annurev-earth-071719-055228

Alabbad, Y., Yildirim, E., & Demir, I. (2023). A web-based analytical urban flood damage and loss estimation framework. *Environmental Modelling & Software*, 163, 105670.

Alabbad, Y., Mount, J., Campbell, A. M., & Demir, I. (2024). A web-based decision support framework for optimizing road network accessibility and emergency facility allocation during flooding. *Urban Informatics*, *3*(1), 10.

Allen, Myles R., and William J. Ingram. "Constraints on future changes in climate and the hydrologic cycle." *Nature* 419.6903 (2002): 224-232. https://doi.org/10.1038/nature01092

Bakanoğulları, F., Şaylan, L., & Yeşilköy, S. (2022). Effects of phenological stages, growth and meteorological factor on the albedo of different crop cultivars. *Italian Journal of Agrometeorology*, *1*, 23-40. https://doi.org/10.36253/ijam-1445

Baydaroğlu, Ö., & Koçak, K. (2014). SVR-based prediction of evaporation combined with chaotic approach. *Journal of Hydrology*, *508*, 356-363. https://doi.org/10.1016/j.jhydrol.2013.11.008

Baydaroğlu, Ö., Koçak, K., & Duran, K. (2018). River flow prediction using hybrid models of support vector regression with the wavelet transform, singular spectrum analysis and chaotic approach. *Meteorology and Atmospheric Physics*, *130*, 349-359. https://doi.org/10.1007/s00703-017-0518-9

Baydaroğlu, Ö., Muste, M., Cikmaz, A. B., Kim, K., Meselhe, E., & Demir, I. (2024). Coping with Information Extraction from In-Situ Data Acquired in Natural Streams. EarthArxiv, 6585. https://doi.org/10.31223/X5S979

Baydaroğlu, Ö., & Demir, I. (2024). Temporal and spatial satellite data augmentation for deep learning-based rainfall nowcasting. *Journal of Hydroinformatics*, *26*(3), 589-607. https://doi.org/10.2166/hydro.2024.235

Bartsev, S., Saltykov, M., Belolipetsky, P., & Pianykh, A. (2021, February). Imperfection of the convergent cross-mapping method. *In IOP Conference Series: Materials Science and Engineering* (Vol. 1047, No. 1, p. 012081). IOP Publishing. https://doi.org/10.1088/1757-899X/1047/1/01208

Bonotto, G., Peterson, T. J., Fowler, K., & Western, A. W. (2022). Identifying causal interactions between groundwater and streamflow using convergent cross-mapping. *Water Resources Research*, *58*(8), e2021WR030231. https://doi.org/10.1029/2021WR030231

Cambron, T. W., Deines, J. M., Lopez, B., Patel, R., Liang, S. Z., & Lobell, D. B. (2024). Further adoption of conservation tillage can increase maize yields in the western US Corn Belt. *Environmental Research Letters*, *19*(5), 054040. https://doi.org/10.1088/1748-9326/ad3f32

Chen, Z., Wang, W., & Fu, J. (2020). Vegetation response to precipitation anomalies under different climatic and biogeographical conditions in China. *Scientific reports*, *10*(1), 830. https://doi.org/10.1038/s41598-020-57910-1

Cikmaz, B. A., Yildirim, E., & Demir, I. (2023). Flood susceptibility mapping using fuzzy analytical hierarchy process for Cedar Rapids, Iowa. *International journal of river basin management*, 1-13.

EM-DAT, 2024. https://public.emdat.be/ (Last Accessed on July 20, 2024)

Feng, S., Oppenheimer, M., & Schlenker, W. (2015). Weather anomalies, crop yields, and migration in the US corn belt. *NBER Working Paper w17734*.

Gong, C., Yao, D., Zhang, C., Li, W., & Bi, J. (2023). Causal discovery from temporal data: An overview and new perspectives. arXiv preprint arXiv:2303.10112.

Hsieh, C. H., Glaser, S. M., Lucas, A. J., & Sugihara, G. (2005). Distinguishing random environmental fluctuations from ecological catastrophes for the North Pacific Ocean. *Nature*, *435*(7040), 336-340. https://doi.org/10.1038/nature03553

Islam, S. S., Yeşilköy, S., Baydaroğlu, Ö., Yıldırım, E., & Demir, I. (2024). State-level multidimensional agricultural drought susceptibility and risk assessment for agriculturally prominent areas. *International Journal of River Basin Management*, 1-18. https://doi.org/10.1080/15715124.2024.2304546

Javier, P. J. E. (2021). Causal-CCM a Python Implementation of Convergent Cross Mapping. *Causal-CCM a Python Implementation of Convergent Cross Mapping*.

Javier, P. J. E. A., Liponhay, M. P., Dajac, C. V. G., & Monterola, C. P. (2022). Causal network inference in a dam system and its implications on feature selection for machine learning forecasting. *Physica A: Statistical Mechanics and its Applications, 604*, 127893. https://doi.org/10.1016/j.physa.2022.127893

Keppenne, C. L. (1995). An ENSO signal in soybean futures prices. *Journal of Climate, 8*(6), 1685-1689. https://doi.org/10.1175/1520-0442(1995)008%3C1685:AESISF%3E2.0.CO;2

Kimm, H., Guan, K., Gentine, P., Wu, J., Bernacchi, C. J., Sulman, B. N., ... & Lin, C. (2020). Redefining droughts for the US Corn Belt: The dominant role of atmospheric vapor pressure deficit over soil moisture in regulating stomatal behavior of Maize and Soybean. *Agricultural and Forest Meteorology, 287*, 107930. https://doi.org/10.1016/j.agrformet.2020.107930

Kullback, S. (1951). Kullback-leibler divergence.

LeComte, D. (2021). US Weather Highlights 2020: The Most Extreme Year on Record?. *Weatherwise*, *74*(3), 14-25. https://doi.org/10.1080/00431672.2021.1896929

Leonard, M., Westra, S., Phatak, A., Lambert, M., van den Hurk, B., McInnes, K., ... & Stafford-Smith, M. (2014). A compound event framework for understanding extreme impacts. *Wiley Interdisciplinary Reviews: Climate Change*, *5*(1), 113-128. https://doi.org/10.1002/wcc.252

Lesk, C., Anderson, W., Rigden, A., Coast, O., Jägermeyr, J., McDermid, S., ... & Konar, M. (2022). Compound heat and moisture extreme impacts on global crop yields under climate change. *Nature Reviews Earth & Environment, 3*(12), 872-889. https://doi.org/10.1038/s43017-022-00368-8

Letson, D., & McCullough, B. D. (2001). ENSO and soybean prices: Correlation without causality. *Journal of Agricultural and Applied Economics, 33*(3), 513-521. https://doi.org/10.1017/S1074070800020976

Li, Z., & Demir, I. (2022). A comprehensive web-based system for flood inundation map generation and comparative analysis based on height above nearest drainage. *Science of The Total Environment*, 828, 154420.

Lu, J., Qin, T., Yan, D., Lv, X., Yuan, Z., Wen, J., ... & Li, W. (2024). Response of Vegetation to Drought in the Source Region of the Yangtze and Yellow Rivers Based on Causal Analysis. *Remote Sensing*, *16*(4), 630. https://doi.org/10.3390/rs16040630

Massaro, D., Rezaeiravesh, S., & Schlatter, P. (2023). On the potential of transfer entropy in turbulent dynamical systems. *Scientific Reports*, *13*(1), 22344. https://doi.org/10.1038/s41598-023-49747-1

Messmer, M., & Simmonds, I. (2021). Global analysis of cyclone-induced compound precipitation and wind extreme events. *Weather and Climate Extremes*, *32*, 100324. https://doi.org/10.1016/j.wace.2021.100324

Mount, J., Sermet, Y., Jones, C.S., Schilling, K.E., Gassman, P.W., Weber, L.J., Krajewski, W.F. and Demir, I., (2024). An integrated cyberinfrastructure system for water quality resources in the Upper Mississippi River Basin. *Journal of Hydroinformatics*, p.jh2024079.

Mønster, D., Fusaroli, R., Tylén, K., Roepstorff, A., & Sherson, J. F. (2017). Causal inference from noisy time-series data—testing the convergent cross-mapping algorithm in the presence of noise and external influence. *Future Generation Computer Systems*, *73*, 52-62. https://doi.org/10.1016/j.future.2016.12.009

Öz, F. Y., Özelkan, E., & Tatlı, H. (2024). Comparative analysis of SPI, SPEI, and RDI ındices for assessing spatio-temporal variation of drought in Türkiye. *Earth Science Informatics*, 1-33. https://doi.org/10.1007/s12145-024-01401-8

Romano, G., Zia, S., Spreer, W., Sanchez, C., Cairns, J., Araus, J. L., & Müller, J. (2011). Use of thermography for high throughput phenotyping of tropical maize adaptation in water stress. *Computers and Electronics in Agriculture*, *79*(1), 67-74. https://doi.org/10.1016/j.compag.2011.08.011

Runge, J., Petoukhov, V., Donges, J. F., Hlinka, J., Jajcay, N., Vejmelka, M., ... & Kurths, J. (2015). Identifying causal gateways and mediators in complex spatio-temporal systems. *Nature communications*, *6*(1), 8502. https://doi.org/10.1038/ncomms9502

Schreiber, T. (2000). Measuring information transfer. *Physical review letters*, *85*(2), 461. https://doi.org/10.1103/PhysRevLett.85.461

Seneviratne, S., Nicholls, N., Easterling, D., Goodess, C., Kanae, S., Kossin, J., ... & Zwiers, F. W. (2012). Changes in climate extremes and their impacts on the natural physical environment.

Shannon, C. E. (1948). A mathematical theory of communication. *The Bell system technical journal*, *27*(3), 379-423. https://doi.org/10.1002/j.1538-7305.1948.tb01338.x

Sironen, A. (2020). Transfer Entropy and Applications to Ecosystem Atmospheric Data.

Soba, D., Arrese-Igor, C., & Aranjuelo, I. (2022). Additive effects of heatwave and water stresses on soybean seed yield is caused by impaired carbon assimilation at pod formation but not at flowering. *Plant Science*, *321*, 111320. https://doi.org/10.1016/j.plantsci.2022.111320

Sugihara, G., & May, R. M. (1990). Nonlinear forecasting as a way of distinguishing chaos from measurement error in time series. *Nature*, *344*(6268), 734-741. https://doi.org/10.1038/344734a0

Sugihara, G., May, R., Ye, H., Hsieh, C. H., Deyle, E., Fogarty, M., & Munch, S. (2012). Detecting causality in complex ecosystems. *Science*, *338*(6106), 496-500. https://doi.org/10.1126/science.1227079

Sugihara, G. (1994). Nonlinear forecasting for the classification of natural time series. *Philosophical Transactions of the Royal Society of London. Series A: Physical and Engineering Sciences*, *348*(1688), 477-495. https://doi.org/10.1098/rsta.1994.0106

Sugihara, G., Park, J., Deyle, E., Saberski, E., Smith, C., & Ye, H. (2020). Empirical dynamic modeling. The Comprehensive R Archive Network. Tomaru, T., Murakami, H., Niizato, T., Nishiyama, Y., Sonoda, K.

Sun, W., Fleisher, D., Timlin, D., Ray, C., Wang, Z., Beegum, S., & Reddy, V. (2023). Projected long-term climate trends reveal the critical role of vapor pressure deficit for soybean yields in the US Midwest. *Science of the Total Environment*, *878*, 162960. https://doi.org/10.1016/j.scitotenv.2023.162960

Tabari, H. (2020). Climate change impact on flood and extreme precipitation increases with water availability. *Scientific reports*, *10*(1), 13768. https://doi.org/10.1038/s41598-020-70816-2

Takens, F., 1981. Detecting strange attractors in turbulence. In: Rand, D.A, Young, L.S. (Eds.), Lecture Notes in Math. Springer-Verlag, pp. 366–381.

Tanir, T., Yildirim, E., Ferreira, C. M., & Demir, I. (2024). Social vulnerability and climate risk assessment for agricultural communities in the United States. *Science of The Total Environment*, *908*, 168346. https://doi.org/10.1016/j.scitotenv.2023.168346

Tewari, R., Mehlhorn, J. E., Parrott, S. D., & Hill, J. I. (2015). Climatic Variability and crop price trends in west Tennessee: A bivariate granger causality analysis. *European Scientific Journal*.

Tian, J., Wang, G., Xiang, D., Huang, S., & Li, W. (2024). Causality analysis and prediction of riverine algal blooms by combining empirical dynamic modeling and machine learning techniques. *Water Resources Research*, *60*(5), e2023WR036334. https://doi.org/10.1029/2023WR036334

Ting, M., Lesk, C., Liu, C., Li, C., Horton, R. M., Coffel, E. D., ... & Singh, D. (2023). Contrasting impacts of dry versus humid heat on US corn and soybean yields. *Scientific reports*, *13*(1), 710. https://doi.org/10.1038/s41598-023-27931-7

USDA-ERS (2024) https://data.ers.usda.gov/reports.aspx?StateFIPS=19&ID=17854

Van Vliet, M. T., Thorslund, J., Strokal, M., Hofstra, N., Flörke, M., Ehalt Macedo, H., ... & Mosley, L. M. (2023). Global river water quality under climate change and hydroclimatic extremes. *Nature Reviews Earth & Environment*, *4*(10), 687-702. https://doi.org/10.1038/s43017-023-00472-3

Veas, R. E., Ergo, V. V., Vega, C. R., Lascano, R. H., Rondanini, D. P., & Carrera, C. S. (2022). Soybean seed growth dynamics exposed to heat and water stress during the filling period under

field conditions. *Journal of Agronomy and Crop Science*, *208*(4), 472-485. https://doi.org/10.1111/jac.12523

Vicente, R., Wibral, M., Lindner, M., & Pipa, G. (2011). Transfer entropy—a model-free measure of effective connectivity for the neurosciences. *Journal of computational neuroscience*, *30*(1), 45-67. https://doi.org/10.1007/s10827-010-0262-3

Vogel, J., Rivoire, P., Deidda, C., Rahimi, L., Sauter, C. A., Tschumi, E., ... & Zscheischler, J. (2021). Identifying meteorological drivers of extreme impacts: an application to simulated crop yields. *Earth System Dynamics*, *12*, 151–172, https://doi.org/10.5194/esd-12-151-2021

Wilson, A. B., Avila-Diaz, A., Oliveira, L. F., Zuluaga, C. F., & Mark, B. (2022). Climate extremes and their impacts on agriculture across the Eastern Corn Belt Region of the US. *Weather and Climate Extremes*, *37*, 100467. https://doi.org/10.1016/j.wace.2022.100467

World Meteorological Organization. (2012). Standardized precipitation index user guide. *World Meteorological Organization*, *1090*.

Yang, Y., Anderson, M. C., Gao, F., Johnson, D. M., Yang, Y., Sun, L., ... & Moore, C. E. (2021). Phenological corrections to a field-scale, ET-based crop stress indicator: An application to yield forecasting across the US Corn Belt. *Remote Sensing of Environment*, *257*, 112337. https://doi.org/10.1016/j.rse.2021.112337

Ye, H., Deyle, E. R., Gilarranz, L. J., & Sugihara, G. (2015). Distinguishing time-delayed causal interactions using convergent cross mapping. *Scientific reports*, *5*(1), 14750. https://doi.org/10.1038/srep14750

Ye, H., Clark, A., Deyle, E., & Sugihara, G. (2016). rEDM: an R package for empirical dynamic modeling and convergent cross-mapping. cran.r-project.org.

Yeşilköy, S., & Şaylan, L. (2022). Spatial and temporal drought projections of northwestern Turkey. *Theoretical and Applied Climatology*, *149*(1), 1-14. https://doi.org/10.1007/s00704-022-04029-0

Yeşilköy, S., Baydaroğlu, Ö., Singh, N., Sermet, Y., & Demir, I. (2023). A Contemporary Systematic Review of Cyberinfrastructure Systems and Applications for Flood and Drought Data Analytics and Communication. EarthArxiv, 5814. https://doi.org/10.31223/X5937W

Yeşilköy, S., Baydaroğlu, Ö., & Demir, I. (2024). Is snow drought a messenger for the upcoming severe drought period? A case study in the upper Mississippi river basin. *Atmospheric Research*, 309, 107553. https://doi.org/10.1016/j.atmosres.2024.107553

Yeşilköy, S., & Baydaroğlu, Ö. (2024). Spatiotemporal Shift and Heterogeneity of Rain-on-Snow Events. *EarthArXiv eprints*, X5497D. https://doi.org/10.31223/X5497D

Yeşilköy, S., & Demir, I. (2024). Crop yield prediction based on reanalysis and crop phenology data in the agroclimatic zones. *Theoretical and Applied Climatology*. https://doi.org/10.1007/s00704-024-05046-x

Yildirim, E., Just, C., & Demir, I. (2022). Flood risk assessment and quantification at the community and property level in the State of Iowa. *International journal of disaster risk reduction*, *77*, 103106. https://doi.org/10.1016/j.ijdrr.2022.103106

Yildirim, E., Alabbad, Y., & Demir, I. (2023). Non-structural flood mitigation optimization at community scale: Middle Cedar Case Study. *Journal of environmental management*, 346, 119025.

Wang, C., Li, Z., Chen, Y., Ouyang, L., Li, Y., Sun, F., ... & Zhu, J. (2023). Drought-heatwave compound events are stronger in drylands. *Weather and Climate Extremes*, *42*, 100632. https://doi.org/10.1016/j.wace.2023.100632

Zhang, N., & Wang, G. (2021). Detecting time-delayed causal interaction between Northern Hemisphere annular mode and winter surface air temperature over Northeast China: a case study of 2009/2010 winter. *Theoretical and Applied Climatology*, *146*, 1249-1256. https://doi.org/10.1007/s00704-021-03793-9

Zhu, Y., & Ghoshray, A. (2021). Climate Anomalies and Its Impact on US Corn and Soybean Prices.

Zhu, Q., Riley, W., Tang, J., Burrows, S., Harrop, B., Shi, X., ... & Calvin, K. (2023). Present and Future Changes in Land-Atmosphere Coupling of Water and Energy Over Extratropical Forest Regions. *Journal of Geophysical Research: Atmospheres*, *128*(8), e2022JD037887. https://doi.org/10.1029/2022JD037887

8. Appendix

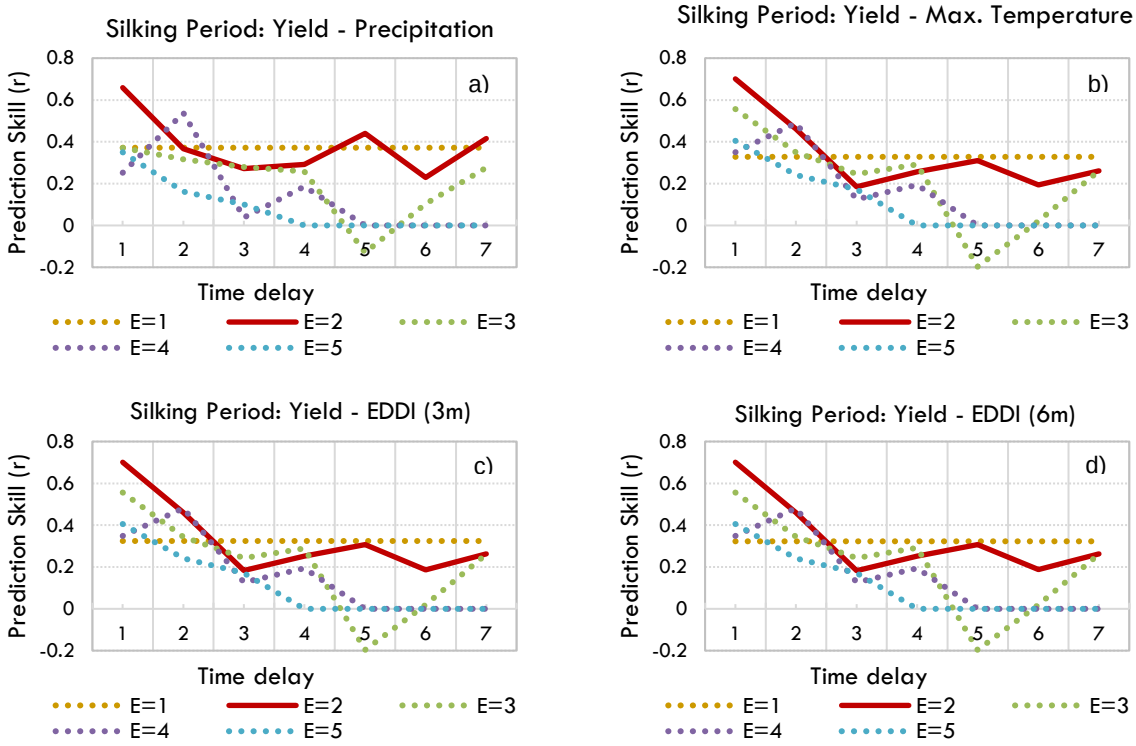

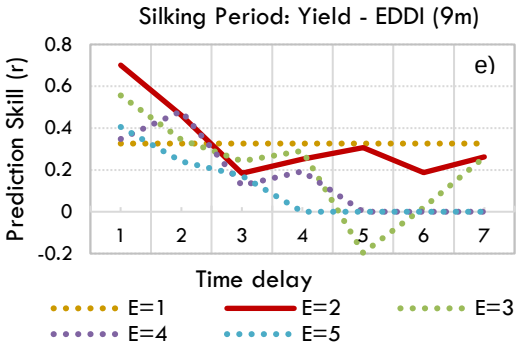
Silking Period: Yield - EDDI (9m)
e)
Prediction Skill (r)
0.8
0.6
0.4
0.2
0
-0.2
1 2 3 4 5 6 7
Time delay
E=1 E=2 E=3
E=4 E=5

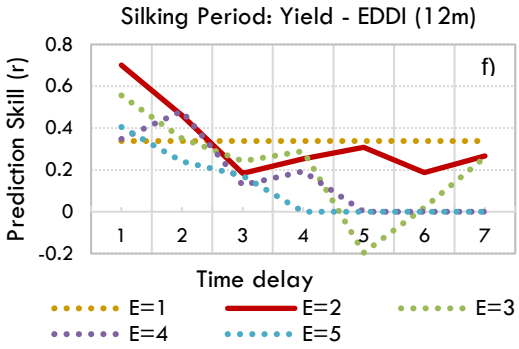
Silking Period: Yield - EDDI (12m)
f)
Prediction Skill (r)
0.8
0.6
0.4
0.2
0
-0.2
1 2 3 4 5 6 7
Time delay
E=1 E=2 E=3
E=4 E=5

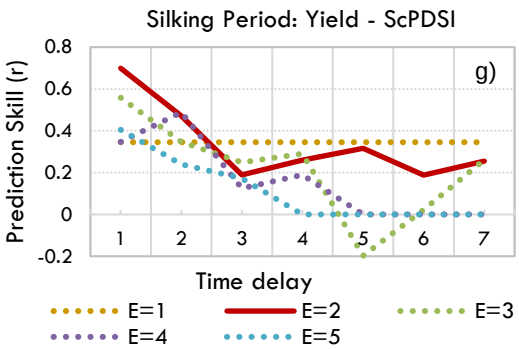
Silking Period: Yield - ScPDSI
g)
Prediction Skill (r)
0.8
0.6
0.4
0.2
0
-0.2
1 2 3 4 5 6 7
Time delay
E=1 E=2 E=3
E=4 E=5

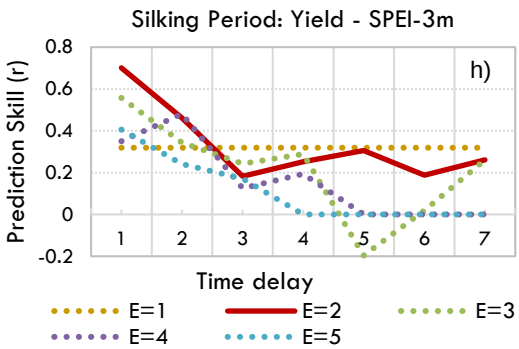
Silking Period: Yield - SPEI-3m
h)
Prediction Skill (r)
0.8
0.6
0.4
0.2
0
-0.2
1 2 3 4 5 6 7
Time delay
E=1 E=2 E=3
E=4 E=5

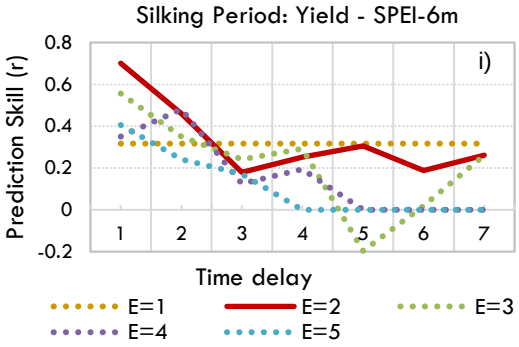
Silking Period: Yield - SPEI-6m
i)
Prediction Skill (r)
0.8
0.6
0.4
0.2
0
-0.2
1 2 3 4 5 6 7
Time delay
E=1 E=2 E=3
E=4 E=5

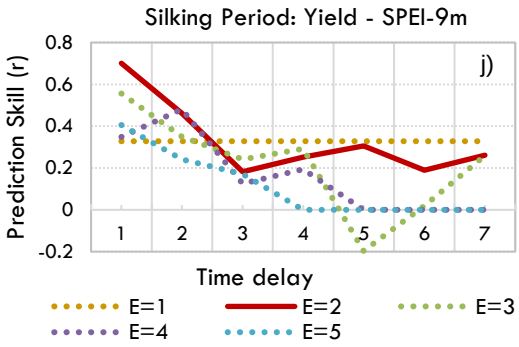
Silking Period: Yield - SPEI-9m
j)
Prediction Skill (r)
0.8
0.6
0.4
0.2
0
-0.2
1 2 3 4 5 6 7
Time delay
E=1 E=2 E=3
E=4 E=5

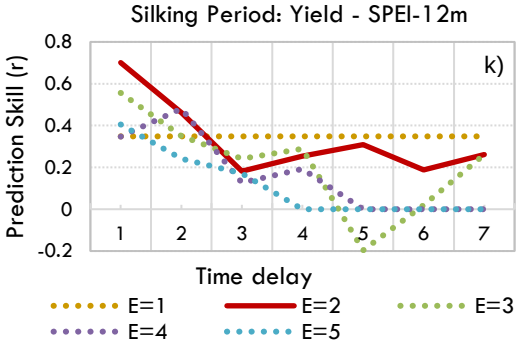
Silking Period: Yield - SPEI-12m
k)
Prediction Skill (r)
0.8
0.6
0.4
0.2
0
-0.2
1 2 3 4 5 6 7
Time delay
E=1 E=2 E=3
E=4 E=5

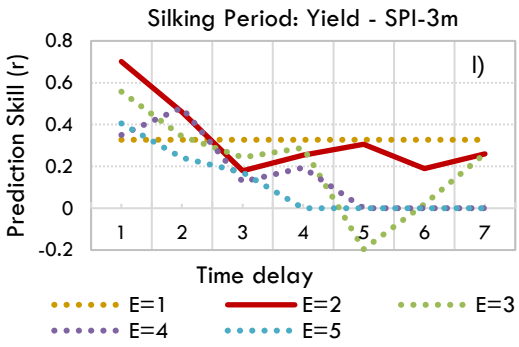
Silking Period: Yield - SPI-3m
l)
Prediction Skill (r)
0.8
0.6
0.4
0.2
0
-0.2
1 2 3 4 5 6 7
Time delay
E=1 E=2 E=3
E=4 E=5

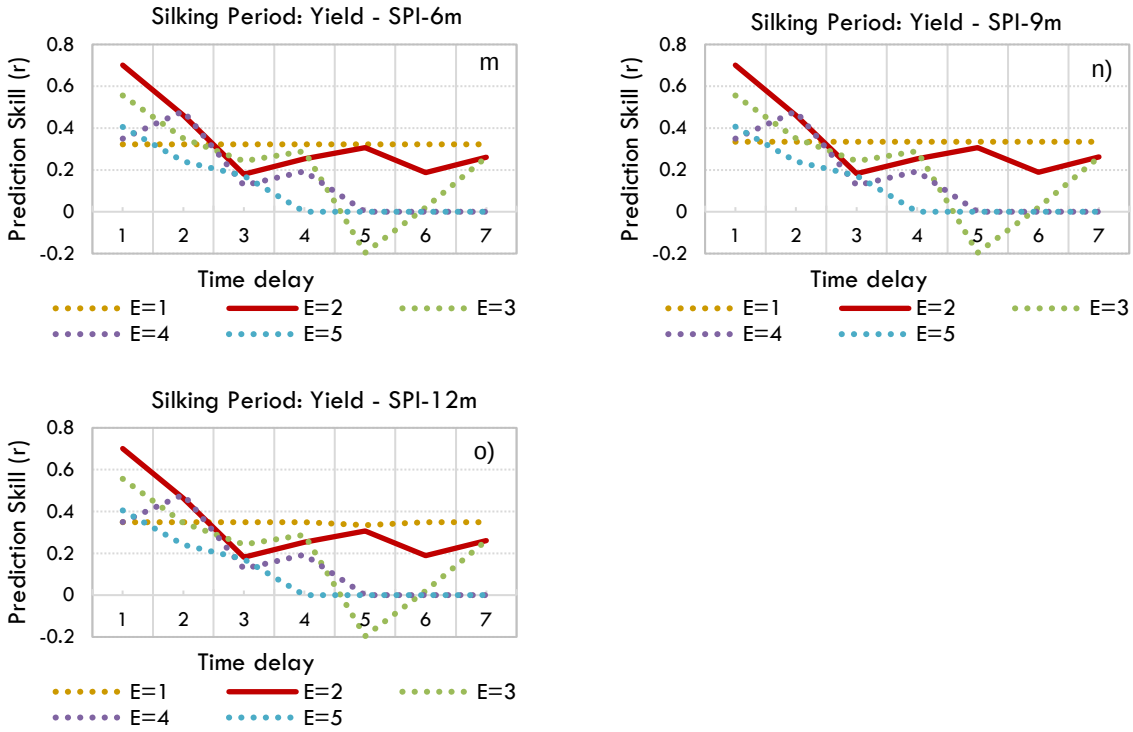

Figure S1. Prediction skill based on time delay and embedding dimension for (a) Precipitation (b) T_{max} (c) EDDI-3m (d) EDDI-6m (e) EDDI-9m (f) EDDI-12m (g) scPDSI (h) SPEI-3m (i) SPEI-6m (j) SPEI-9m (k) SPEI-12m (l) SPI-3m (m) SPI-6m (n) SPI-9m (o) SPI-12m.

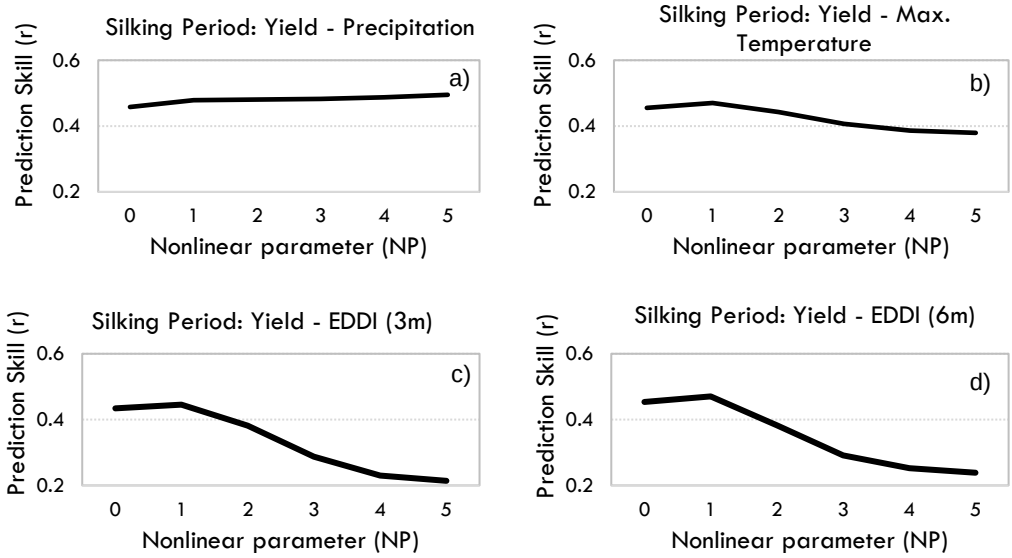

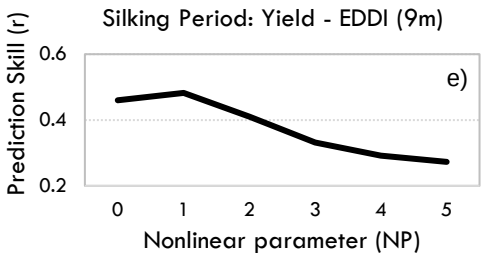
Silking Period: Yield - EDDI (9m)
Prediction Skill (r)
0.6
0.4
0.2
e)
0 1 2 3 4 5
Nonlinear parameter (NP)

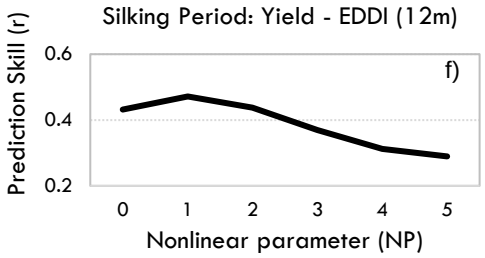
Silking Period: Yield - EDDI (12m)
Prediction Skill (r)
0.6
0.4
0.2
f)
0 1 2 3 4 5
Nonlinear parameter (NP)

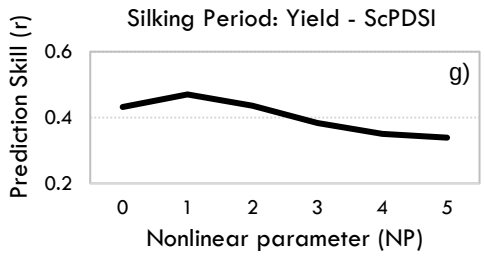
Silking Period: Yield - ScPDSI
Prediction Skill (r)
0.6
0.4
0.2
g)
0 1 2 3 4 5
Nonlinear parameter (NP)

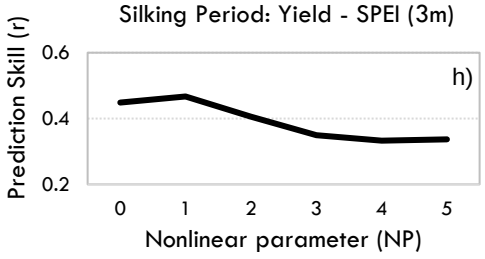
Silking Period: Yield - SPEI (3m)
Prediction Skill (r)
0.6
0.4
0.2
h)
0 1 2 3 4 5
Nonlinear parameter (NP)

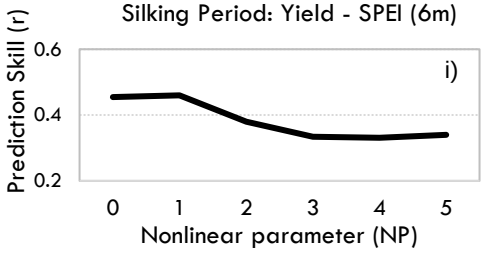
Silking Period: Yield - SPEI (6m)
Prediction Skill (r)
0.6
0.4
0.2
i)
0 1 2 3 4 5
Nonlinear parameter (NP)

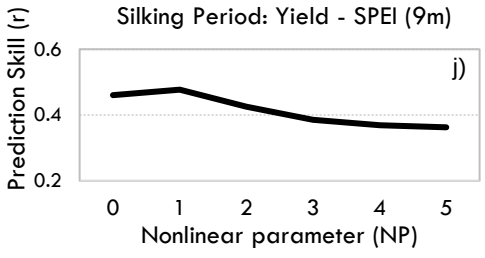
Silking Period: Yield - SPEI (9m)
Prediction Skill (r)
0.6
0.4
0.2
j)
0 1 2 3 4 5
Nonlinear parameter (NP)

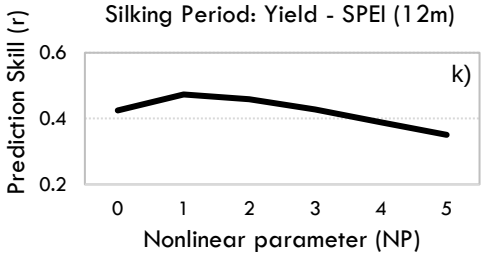
Silking Period: Yield - SPEI (12m)
Prediction Skill (r)
0.6
0.4
0.2
k)
0 1 2 3 4 5
Nonlinear parameter (NP)

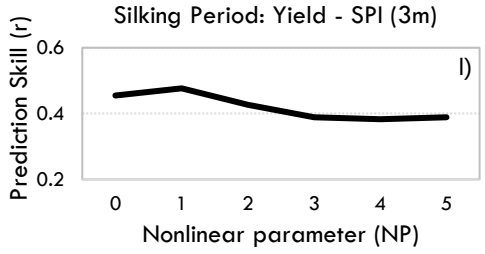
Silking Period: Yield - SPI (3m)
Prediction Skill (r)
0.6
0.4
0.2
l)
0 1 2 3 4 5
Nonlinear parameter (NP)

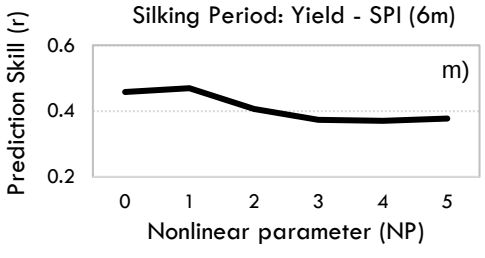
Silking Period: Yield - SPI (6m)
Prediction Skill (r)
0.6
0.4
0.2
m)
0 1 2 3 4 5
Nonlinear parameter (NP)

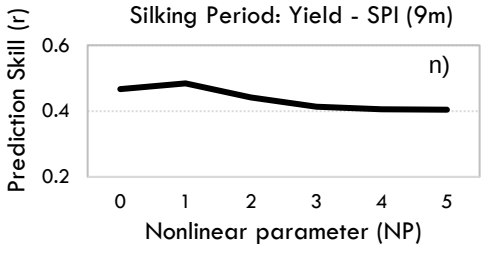
Silking Period: Yield - SPI (9m)
Prediction Skill (r)
0.6
0.4
0.2
n)
0 1 2 3 4 5
Nonlinear parameter (NP)

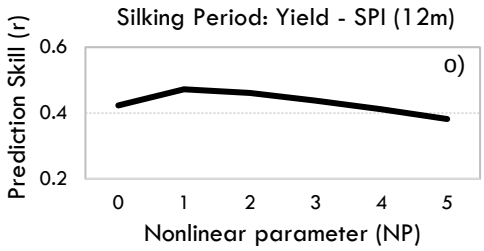

Figure S2. Prediction skill based on nonlinear parameter for (a) Precipitation (b) T_{max} (c) EDDI-3m (d) EDDI-6m (e) EDDI-9m (f) EDDI-12m (g) scPDSI (h) SPEI-3m (i) SPEI-6m (j) SPEI-9m (k) SPEI-12m (l) SPI-3m (m) SPI-6m (n) SPI-9m (o) SPI-12m.

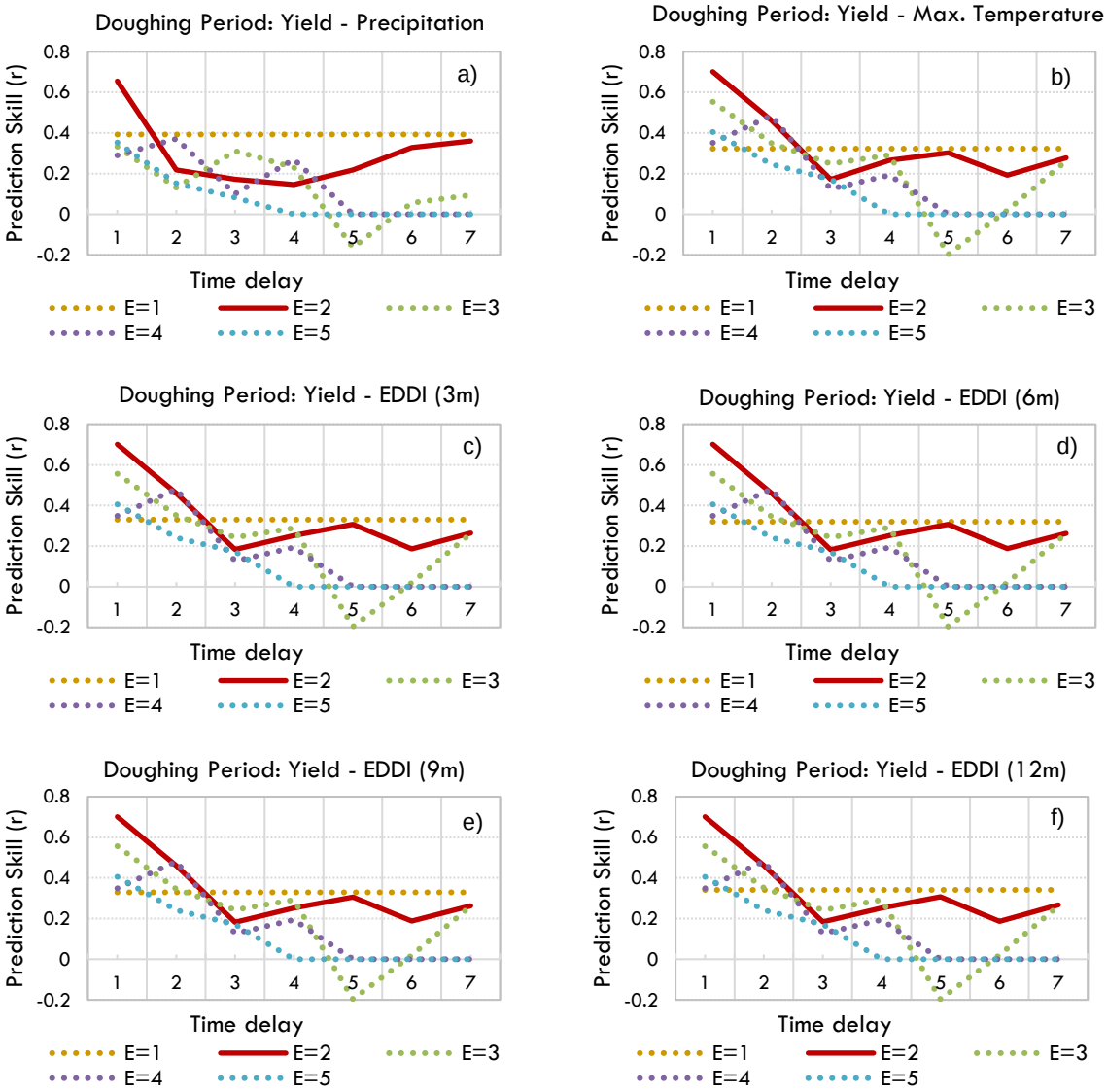

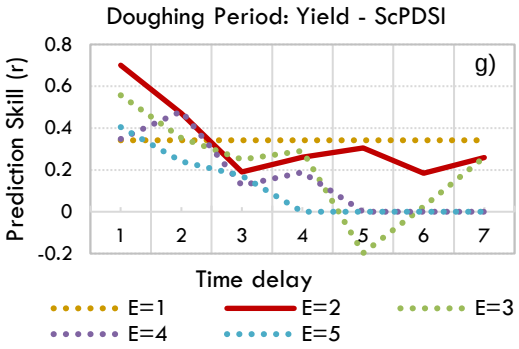
Doughing Period: Yield - ScPDSI
g)
Prediction Skill (r)
0.8
0.6
0.4
0.2
0
-0.2
1 2 3 4 5 6 7
Time delay
E=1 E=2 E=3
E=4 E=5

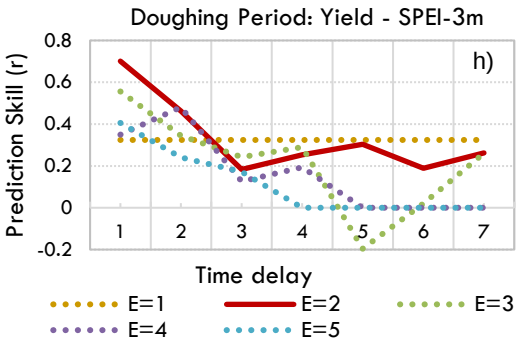
Doughing Period: Yield - SPEI-3m
h)
Prediction Skill (r)
0.8
0.6
0.4
0.2
0
-0.2
1 2 3 4 5 6 7
Time delay
E=1 E=2 E=3
E=4 E=5

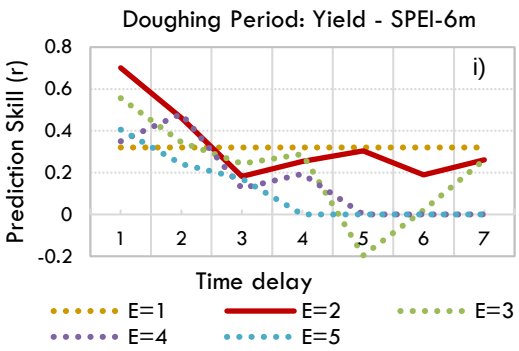
Doughing Period: Yield - SPEI-6m
i)
Prediction Skill (r)
0.8
0.6
0.4
0.2
0
-0.2
1 2 3 4 5 6 7
Time delay
E=1 E=2 E=3
E=4 E=5

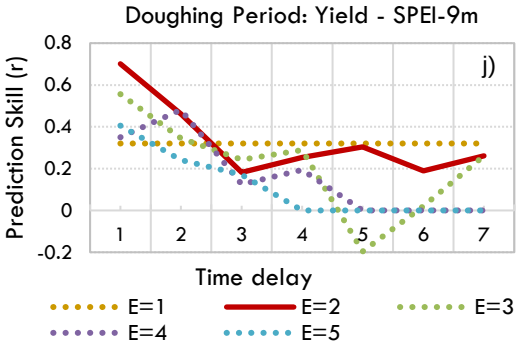
Doughing Period: Yield - SPEI-9m
j)
Prediction Skill (r)
0.8
0.6
0.4
0.2
0
-0.2
1 2 3 4 5 6 7
Time delay
E=1 E=2 E=3
E=4 E=5

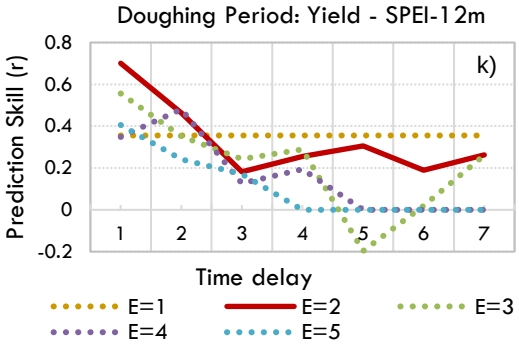
Doughing Period: Yield - SPEI-12m
k)
Prediction Skill (r)
0.8
0.6
0.4
0.2
0
-0.2
1 2 3 4 5 6 7
Time delay
E=1 E=2 E=3
E=4 E=5

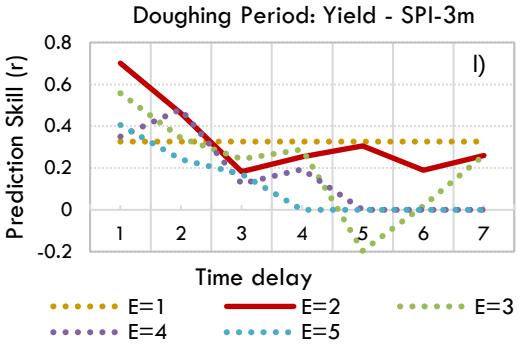
Doughing Period: Yield - SPI-3m
l)
Prediction Skill (r)
0.8
0.6
0.4
0.2
0
-0.2
1 2 3 4 5 6 7
Time delay
E=1 E=2 E=3
E=4 E=5

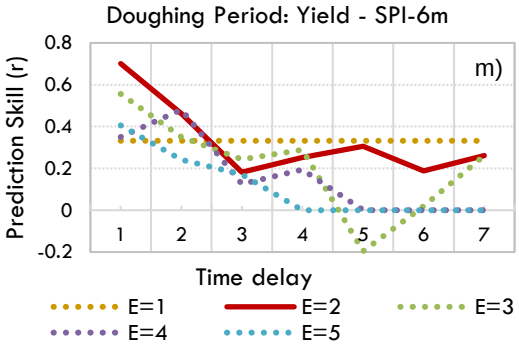
Doughing Period: Yield - SPI-6m
m)
Prediction Skill (r)
0.8
0.6
0.4
0.2
0
-0.2
1 2 3 4 5 6 7
Time delay
E=1 E=2 E=3
E=4 E=5

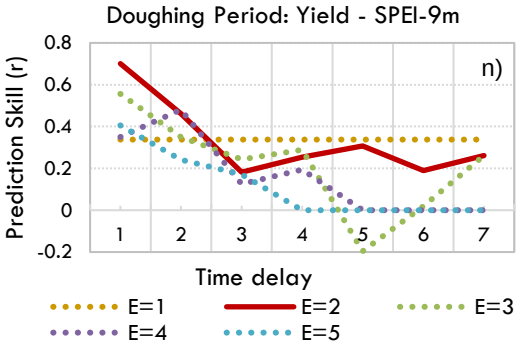
Doughing Period: Yield - SPEI-9m
n)
Prediction Skill (r)
0.8
0.6
0.4
0.2
0
-0.2
1 2 3 4 5 6 7
Time delay
E=1 E=2 E=3
E=4 E=5

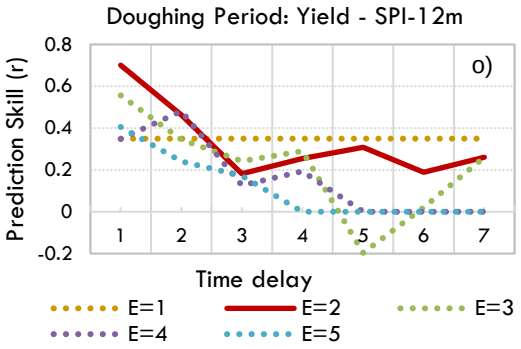

Figure S3. Prediction skill based on time delay and embedding dimension for (a) Precipitation (b) T_{max} (c) EDDI-3m (d) EDDI-6m (e) EDDI-9m (f) EDDI-12m (g) scPDSI (h) SPEI-3m (i) SPEI-6m (j) SPEI-9m (k) SPEI-12m (l) SPI-3m (m) SPI-6m (n) SPI-9m (o) SPI-12m.

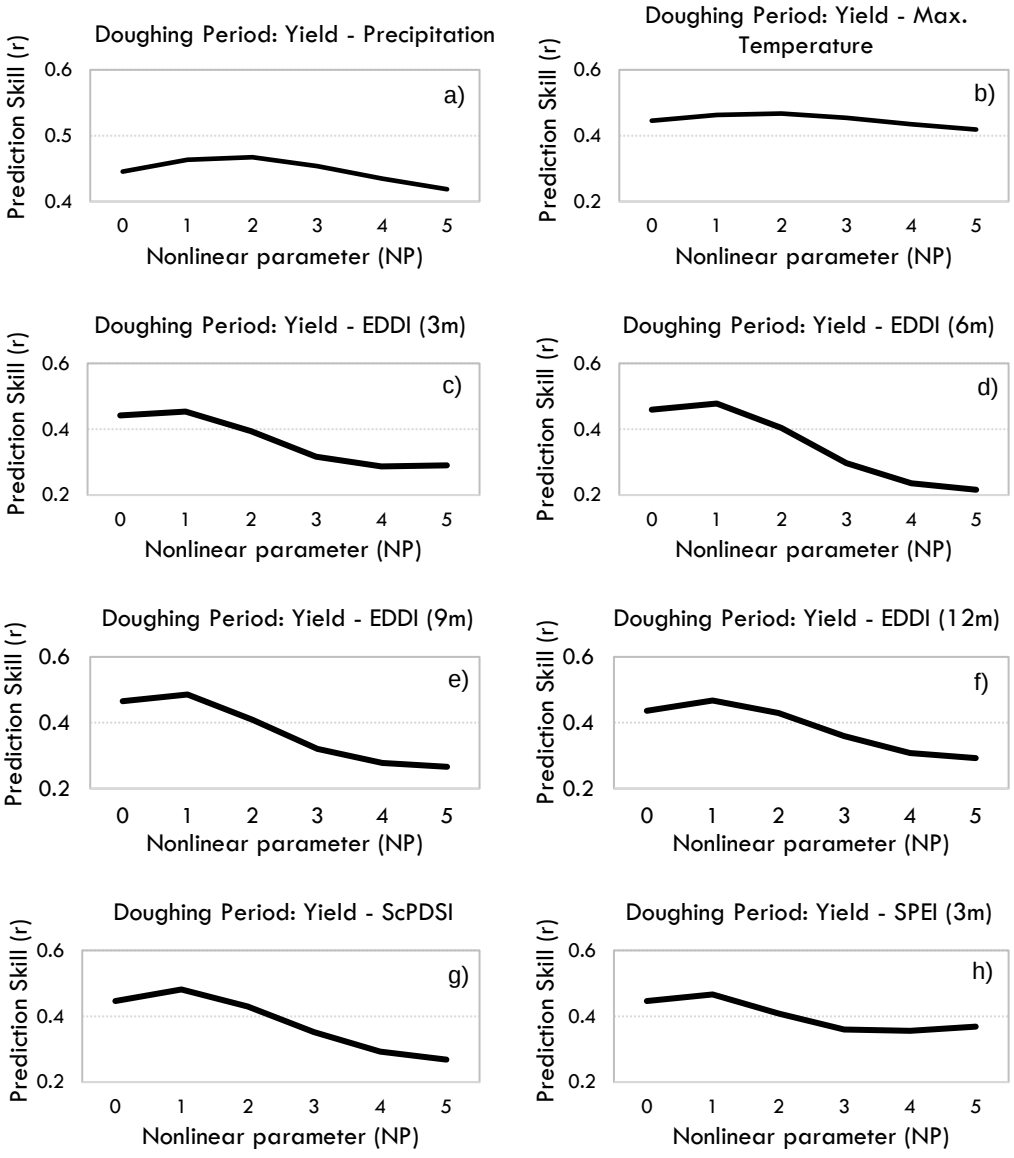

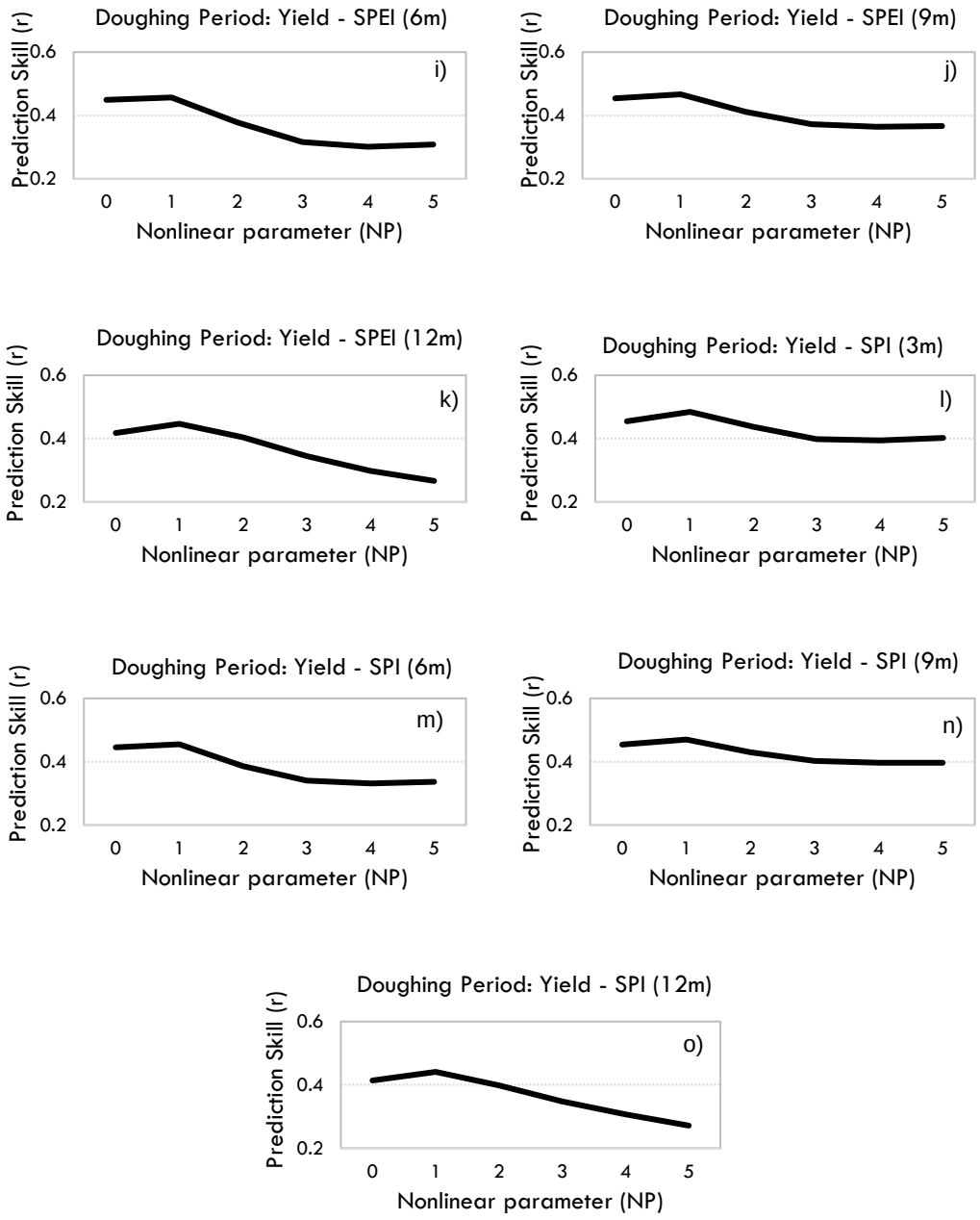

Figure S4. Prediction skill based on nonlinear parameter for (a) Precipitation (b) T_{max} (c) EDDI-3m (d) EDDI-6m (e) EDDI-9m (f) EDDI-12m (g) scPDSI (h) SPEI-3m (i) SPEI-6m (j) SPEI-9m (k) SPEI-12m (l) SPI-3m (m) SPI-6m (n) SPI-9m (o) SPI-12m.